Effects of Dual-energy Subtraction Chest Radiography on Detection of Small Pulmonary Nodules with Various Attenuation: Receiver Operating Characteristics Analysis by Using Phantom Study

ABSTRACT

Purpose: To investigate the detectability of simulated pulmonary nodules with different X-ray attenuation by flat-panel detector (FPD) chest radiography using a dual-exposure dual-energy subtraction (DES) technique.

Materials and Methods: Using a FPD radiography system we obtained 108 sets of chest radiographs of a chest phantom. They consisted of 54 sets each of chest radiographs with- and without simulated nodules. Each data set contained a standard- and a corresponding dual-energy subtracted chest radiograph (DES image). The diameter of the simulated nodules was 8-, 10-, and 12 mm; nodules of each size manifested attenuation of -450, -200, and 30 Hounsfield units (HU). We performed receiver operating characteristic (ROC) analysis to compare the observers' performance in detecting nodules.

Results: For -450 HU nodules the mean area under the ROC curve (AUC) without and with DES images was 0.66 and 0.77, respectively; the difference was significant (paired t-test, $p < 0.01$). For nodules with -200- and 30 HU, there was no significant difference in the AUC value (0.79 vs. 0.77, $p=0.13$; 0.92 vs. 0.94, $p=0.17$, respectively).

Conclusion: The addition of DES images to standard chest radiographs improved the

performance of radiologists charged with detecting simulated nodules with an attenuation of -450 HU.

Key words

dual-energy subtraction, flat-panel detector, chest radiography, ROC analysis, phantom

INTRODUCTION

Chest radiography still represents the most common tool in diagnostic radiology due to its low cost, low dose, and simple implementation. However, the false-negative rate of chest radiography for the detection of pulmonary nodules is relatively high; it was reported to range from 19 to 72 % (1, 2). The failure to detect pulmonary nodules on chest radiographs has been attributed to their size (3) and density (4) and obscuration by bony structures such as the ribs and/or clavicles (5). The dual-energy subtraction (DES) technique for chest radiography is one of the promising methods to reduce these anatomical noises. Using different energy X-ray beams, DES chest radiography can remove overlying bone structures and generate soft-tissue-selective images (6, 7). It enhances the visualization of pulmonary nodules overlaid by bones and may improve the detectability of pulmonary nodules. The DES technique is now available in full-field digital flat-panel detector (FPD) radiography systems that feature rapid accessibility of images, improved image quality, and the possibility of reduced radiation exposure (8).

The aim of this study was to investigate the detectability of simulated pulmonary nodules with different X-ray attenuation by FPD chest radiography using a dual-exposure DES technique.

MATERIALS AND METHODS

Dual-Energy Subtraction Chest Radiography

DES chest radiographs were obtained using a FPD digital chest system (Revolution XR/d, GE Healthcare, Milwaukee, WI). The detector featured an image size of 41 × 41 cm and a pixel dimension of 0.2 ×0.2 mm. DES images were acquired with a double-exposure technique with 200 ms between the high- (120-kV) and low-energy (60-kV) exposures; standard posteroanterior-, soft-tissue-, and bone images were generated. The imaging parameters included a 120-kV image at a speed equivalent to approximately 400, and a 60-kV image at a speed setting equivalent to approximately 1000. Our phantom study had shown that the entrance surface radiation dose for a standard posteroanterior chest radiograph with the FPD system was 0.097 mGy; it was 0.168 mGy for double-exposure DES imaging at the above speed setting (unpublished data). The radiation dose at double-exposure DES chest radiography with the FPD system is nearly equal to that of conventional computed- or film-screen radiography systems (8) and lower than that of the International Atomic Energy Agency (IAEA) guidance level for diagnostic chest radiography, i.e. 0.4 mGy at posteroanterior chest radiography (9).

Database

We used a chest phantom and simulated nodules (multi-purpose chest phantom N1, Kyoto Kagaku Co., Kyoto, Japan). In this phantom, simulated soft tissues such as pulmonary vessels, the chest wall, heart, diaphragm, and liver consist of polyurethane resin composites; simulated bone of an epoxide resin. The space between the pulmonary vessels, heart, and chest wall was filled with air. The chest wall can be removed from the other structures such as the simulated heart, pulmonary vessels, diaphragm, and liver. Simulated nodules were spheres made of urethane foam resin. We arbitrarily placed nodules on the bifurcations of the pulmonary vessels at any level of the lungs.

Using an FPD radiography system, we obtained 108 sets of chest radiographs of a chest phantom which consisted of 54 sets each of chest radiographs with- and without simulated pulmonary nodules. Each data set also contained a standard- and a corresponding dual-energy subtracted chest radiograph (DES image). The diameter of the simulated nodules was 8-, 10-, and 12 mm; nodules of each size manifested attenuation of -450, -200, and 30 Hounsfield units (HU, nominal values), the actual values measured at our CT scanners were -443, -205, 33 HU, respectively. The simulated nodules were randomly inserted into the lung field of the chest phantom by

one of the authors (Y. F.) who did not participate the observer performance study.

Observer Performance Study

We used a sequential-test method for receiver-operating-characteristic (ROC) analysis to evaluate the diagnostic performance of radiologists detecting pulmonary nodules on chest radiographs without and with DES images. Seven board-certified radiologists with 10 – 22 years of experience (mean 13.3 years) participated in this observer performance study. All specialized in body imaging and read chest radiographs regularly. They were allowed to change the level and width of the window on the monitor; reading time was not limited.

All observers recorded the location of detected simulated nodules on record sheets. They used a continuous rating scale and a line-marking method to rate their confidence level by placing marks on a 7-cm-long line on a recording form. The left end of the line indicated complete confidence that the chest radiographs without/with DES images did not, the right end indicated complete confidence that they did reveal a nodule. Intermediate levels of confidence were indicated by the position of the marks between the 2 line termini, where marks close to the right and left end indicated a greater and lesser degree of confidence, respectively. One author (Y.F.) then measured the distance between the left end of the line and the mark and converted the

distance to an ordinal confidence rating ranging from 0 - 100. A continuous rating scale containing a pair of horizontal lines was used in the sequential test. Observers first recorded their rating of chest radiographs without DES images on the upper line. Subsequently, they recorded their rating of DES images on the lower line. They entered their results for each case on a record form.

Statistical Analysis

We used ROC analysis to compare the radiologists' performance in detecting simulated pulmonary nodules with the different attenuation values on chest images acquired without and with the DES technique. A binormal ROC curve was fitted to each radiologist's confidence rating data acquired under the 2 reading conditions by applying quasi-maximum likelihood estimation (10). A computer program (ROCKIT; Charles E. Metz, University of Chicago, Chicago, IL) was used for obtaining binormal ROC curves from the ordinal-scale rating data (10). The area under the best-fit ROC curve (AUC) plotted in unit squares was calculated for each fitted curve.

The statistical significance of the difference in AUC values between the ROC curves obtained without and with DES images was tested. The paired t-test was performed with a statistical software package (SPSS, version 15.0; SPSS, Chicago, IL),

and p values less than 0.05 were considered to indicate statistically significant differences.

RESULTS

For all simulated nodules the AUC values for all 7 observers were higher with than without DES images (Table 1). Analysis of the overall performance of the 7 observers in the detection of simulated nodules indicated that the mean AUC values increased from 0.76 ± 0.08 (without DES images) to 0.79 ± 0.07 (with DES images); the difference was statistically significant ($p = 0.02$) (Fig. 1).

For simulated -450 HU nodules the mean AUC vales without and with DES images were 0.66 ± 0.06 and 0.77 ± 0.03, respectively; the difference was statistically significant ($p < 0.01$) (Fig. 2). On the other hand, for simulated nodules with -200- and 30 HU, there was no statistically significant difference in the AUC values without and with DES images (0.79 ± 0.07 vs. 0.77 ± 0.07, $p=0.13$; 0.92 ± 0.04 vs. 0.94 ± 0.03, $p=0.17$, respectively) (Figs. 3, 4).

When an observer correctly identified the location of the nodules and assigned a confidence level of 50 or more, we recorded the diagnosis as being correct and calculated mean sensitivity, specificity, accuracy, and positive- and negative predictive values (PPV, NPV) for all observers for all nodules. The sensitivity, specificity, accuracy, PPV, and NPV were 48.8%, 83.6%, 65.4%, 79.5%, and 58.9%, respectively, for standard images. These values were 63.2%, 83.6%, 73.4%, 82.6%, and 70.6%,

respectively, for DES images (Table 2). On DES images, sensitivity, accuracy and NPV were significantly improved.

A representative case is shown in Fig. 5.

DISCUSSION

Chest radiography is currently the most frequently used screening procedure for lung cancer because it is economical and easy to use. One of the main shortcomings of chest radiography is poor sensitivity for the detection of solitary pulmonary nodules that are smaller than 2 cm in diameter (11). Furthermore, the detection of small ground glass opacity (GGO) nodules is especially difficult on chest radiographs.

Results of previous studies indicated the usefulness of the DES technique at computed radiography or on film-screen systems (12). Few earlier studies evaluated the performance of radiologists in the detection of pulmonary nodules using DES techniques with the FPD system and the usefulness of this technique with the FPD system has not been established. Tagashira et al. (13) studied 50 patients with one or more nodules and 50 patients without nodules; they reported that the AUC values of 7 observers were significantly increased from 0.79 to 0.84 with DES images. Ricke et al. (14) evaluated 20 patients with a total of 59 pulmonary nodules; they found that the DES technique significantly improved sensitivity (from 33 to 42%), specificity (from 81 to 85%), and confidence in the detection of small pulmonary nodules. On the other hand, Rühl et al. (15), who studied 100 patients with a total of 149 pulmonary nodules, concluded that at FPD chest radiography the DES technique did not

significantly improve the detection of pulmonary nodules. However, they did not analyze the relationship between nodule detectability and nodule density. Our study is the first to investigate the detection of pulmonary nodules from the viewpoint of their relationship to nodule density using the DES technique with the FPD radiography system.

Our results suggested that the combined evaluation of DES images and original chest radiographs significantly improved the diagnostic performance of observers in the detection of simulated nodules with an attenuation of -450 HU but not of -200- and 30 HU. We posit that DES images enhance the visualization of pulmonary nodules with -450 HU, especially of nodules with overlapping bone shadows. Consequently, the detectability of nodules with -450 HU was improved.

Ide et al. (6) who studied 77 consecutive lung cancer patients and 77 healthy subjects reported that the DES technique at computed radiography failed to improve the detection of non-solid- and solid nodules, however, it significantly improved the detection of part-solid nodules, all of which were bronchioloalveolar carcinoma. We posit that -450 HU is equivalent to the density of part-solid nodules from bronchioloalveolar carcinoma (16).

The DES technique with the FPD system may also improve the detectablity of

part-solid nodules. On the other hand, the detectability of -200- and 30 HU nodules was equivalent on DES- and standard images.

FPD radiography systems are now widely used because of the rapid accessibility of images, improved image quality, and the possibility of reduced radiation exposure (8). The FDP radiography system yields higher detective quantum efficiency (DQE) than computed radiography and film-screen radiography systems (17). A higher DQE increases the ability to reveal objects in a noisy background (17) and reduces the radiation exposure without sacrificing image quality. At approximately 50% of the radiation dose, the quality of images obtained with the FPD radiography system was equal to that of computed- or film-screen radiography systems (18) and use of the double-exposure technique with FPD may not increase the radiation dose compared with these other systems.

Currently, single- and double-exposure dual-energy systems are available. In the former, DES images are obtained by exposing two storage phosphor plates separated by a copper filter. A disadvantage is the lower signal-to-noise ratio of the tissue-selective subtraction image. Also, theoretically, single-exposure systems cannot be used with FPD systems. On the other hand, in double-exposure systems (7), two sequential radiographs are obtained at low- and high kV settings, respectively.

The 200-millisecond delay between the two exposures may produce misregistration artifacts on the subtracted images. However, double-exposure systems produce DES images with a better signal-to-noise ratio than single-exposure systems.

There are several limitations in our study. First, we did not evaluate the effect of this technique on the efficacy of detecting pulmonary nodules with calcification. While such nodules may be subtracted on soft tissue images, they can be detected easily on standard- or bone images. Since most calcified nodules are benign, their detection may be of lower clinical significance. Second, we only evaluated the detectability of pulmonary nodules. We did not distinguish between nodules obscured by clavicles or ribs as compared to nodules not overlaid by structures that are subtracted by the DES technique. However, we analyzed the relationship between nodule detectability and bony structures in an unpublished clinical study. We found that diagnostic performance was significantly improved for nodules with overlapping bone shadows, for nodules without overlapping, it was not. Furthermore, Kido et al. (19,20), who studied single-exposure DES images using computed radiography, revealed that DES images especially improved the detectability of nodules with overlapping bone shadows. Third, we conducted only phantom- but not clinical studies. The simulated nodules in the chest phantom were round and had

clear margins and there were no misregistration artifacts such as may be attributable to cardiac-, respiratory-, and patient motion in the clinical setting where pulmonary nodules are not necessarily round, their margins are not always clear, and there may be various lung diseases in the patient background. In addition, misregistration artifacts may be present on clinical images. Therefore, the detection of small pulmonary nodules on DES images may be more difficult in clinical- than phantom studies. The DES technique should be rigorously evaluated by large-scale clinical studies. Finally, this technique should also be evaluated with respect to the nodule size and the observers' experience with the interpretation of chest radiographs.

In conclusion, the addition of DES images to standard chest radiographs improved the performance of radiologists charged with detecting simulated nodules with an attenuation of -450 HU. The detectability of -200-, 0-, and 30 HU nodules was equivalent on DES- and standard images. We suggest that the DES technique with FPD chest radiography can reduce the number of GGO nodules that are missed in routine clinical practice.

REFERENCES

1. Kaneko M, Eguchi K, Ohmatsu H, et al. Peripheral lung cancer: Screening and detection with low-dose spiral CT versus radiography. Radiology 1996; 201:798-802.

2. Quekel LG, Kessels AG, Goei R, van Engelshoven JM. Miss rate of lung cancer on the chest radiograph in clinical practice. Chest 1999; 115:720-724.

3. Woodring JH. Pitfalls in the radiologic diagnosis of lung cancer. AJR Am J Roentgenol 1990; 154:1165-1175.

4. Tsubamoto M, Kuriyama K, Kido S, et al. Detection of lung cancer on chest radiographs: Analysis on the basis of size and extent of ground-glass opacity at thin-section CT. Radiology 2002; 224:139-144.

5. Shah PK, Austin JH, White CS, et al. Missed non-small cell lung cancer: Radiographic findings of potentially resectable lesions evident only in retrospect. Radiology 2003; 226:235-241.

6. Ide K, Mogami H, Murakami T, Yasuhara Y, Miyagawa M, Mochizuki T. Detection of lung cancer using single-exposure dual-energy subtraction chest radiography. Radiat Med 2007; 25:195-201.

7. Uemura M, Miyagawa M, Yasuhara Y, et al. Clinical evaluation of pulmonary

nodules with dual-exposure dual-energy subtraction chest radiography. Radiat Med 2005; 23:391-397.

8. Bacher K, Smeets P, Bonnarens K, De Hauwere A, Verstraete K, Thierens H. Dose reduction in patients undergoing chest imaging: Digital amorphous silicon flat-panel detector radiography versus conventional film-screen radiography and phosphor-based computed radiography. AJR Am J Roentgenol 2003; 181:923-929.

9. International Atomic Energy Agency. International basic safety standards for protection against ionizing radiation and for the safety of radiation sources. IAEA safety series no. 115. Vienna, Austria: International Atomic Energy Agency, 1996.

10. Metz CE, Herman BA, Shen JH. Maximum likelihood estimation of receiver operating characteristic (ROC) curves from continuously-distributed data. Stat Med 1998; 17:1033-1053.

11. Shiraishi J, Katsuragawa S, Ikezoe J, et al. Development of a digital image database for chest radiographs with and without a lung nodule: Receiver operating characteristic analysis of radiologists' detection of pulmonary nodules. AJR Am J Roentgenol 2000; 174:71-74.

12. Kelcz F, Zink FE, Peppler WW, Kruger DG, Ergun DL, Mistretta CA. Conventional chest radiography vs dual-energy computed radiography in the detection and characterization of pulmonary nodules. AJR Am J Roentgenol 1994; 162:271-278.

13. Tagashira H, Arakawa K, Yoshimoto M, Mochizuki T, Murase K. Detectability of lung nodules using flat panel detector with dual energy subtraction by two shot method: Evaluation by ROC method. Eur J Radiol 2007; 64:279-284.

14. Ricke J, Fischbach F, Freund T, et al. Clinical results of CsI-detector-based dual-exposure dual energy in chest radiography. Eur Radiol 2003; 13:2577-2582.

15. Ruhl R, Wozniak MM, Werk M, et al. CsI-detector-based dual-exposure dual energy in chest radiography for lung nodule detection: Results of an international multicenter trial. Eur Radiol 2008; 18:1831-1839.

16. Oda S, Awai K, Liu D, et al. Ground-glass opacities on thin-section helical CT: Differentiation between bronchioloalveolar carcinoma and atypical adenomatous hyperplasia. AJR Am J Roentgenol 2008; 190:1363-1368.

17. Floyd CE, Jr., Warp RJ, Dobbins JT, 3rd, et al. Imaging characteristics of an amorphous silicon flat-panel detector for digital chest radiography. Radiology

2001; 218:683-688.

18. Hamer OW, Volk M, Zorger Z, Feuerbach S, Strotzer M. Amorphous silicon, flat-panel, x-ray detector versus storage phosphor-based computed radiography: Contrast-detail phantom study at different tube voltages and detector entrance doses. Invest Radiol 2003; 38:212-220.

19. Kido S, Ikezoe J, Naito H, et al. Single-exposure dual-energy chest images with computed radiography. Evaluation with simulated pulmonary nodules. Invest Radiol 1993; 28:482-487.

20. Kido S, Ikezoe J, Naito H, et al. Clinical evaluation of pulmonary nodules with single-exposure dual-energy subtraction chest radiography with an iterative noise-reduction algorithm. Radiology 1995; 194:407-412.

FIGURE

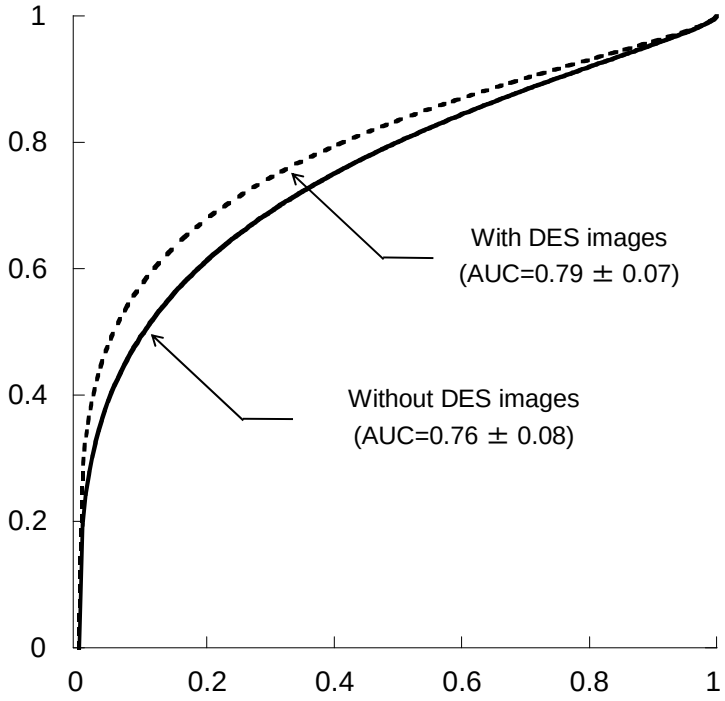

Fig. 1 - ROC curves of the diagnostic performance of all observers without and with DES images. The average AUC value is significantly improved with DES images ($p = 0.02$).

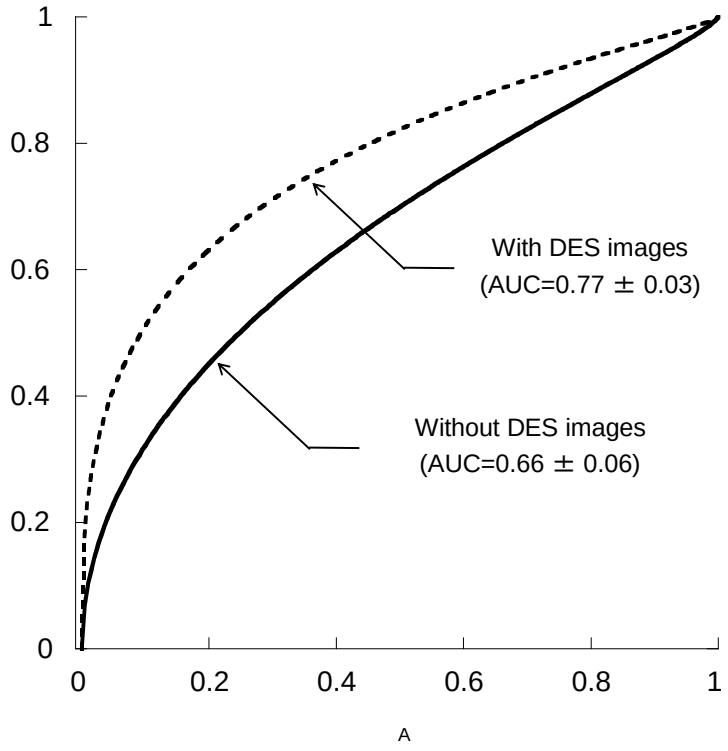

Fig. 2 – ROC curves of the diagnostic performance of all observers for -450 HU nodules without and with DES images. The average AUC value is significantly improved with DES images ($p < 0.01$).

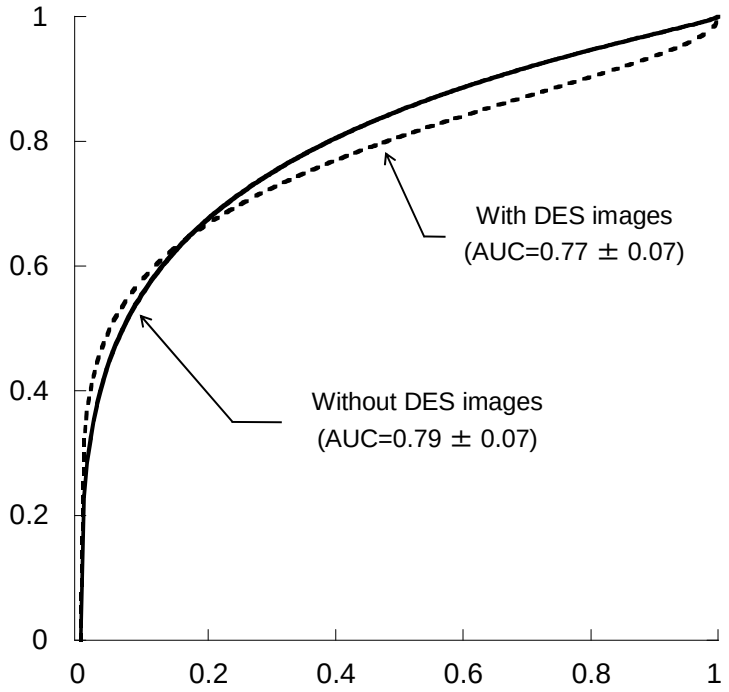

Fig. 3 – ROC curves of the diagnostic performance of all observers for -200 HU nodules. There was no statistically significant difference in the AUC values without and with DES (p=0.13).

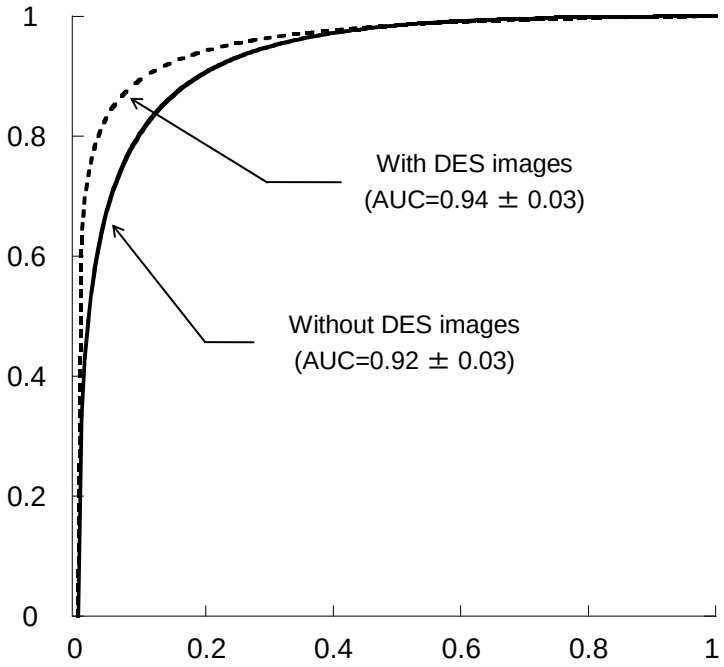

Fig. 4 – ROC curves of the diagnostic performance of all observers for 30-HU nodules. There was no statistically significant difference in the AUC values without and with DES (p=0.17).

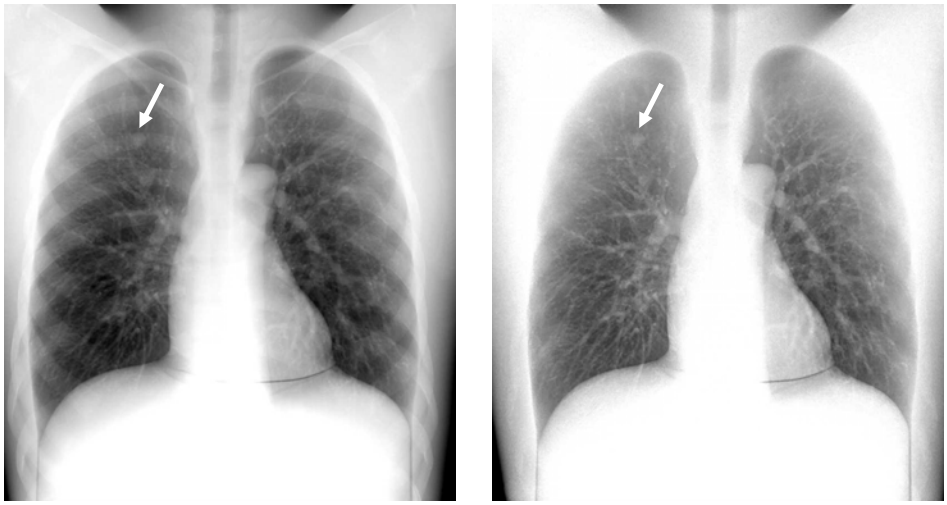

a **b**

Fig. 5 – Chest phantom with a simulated -450 HU nodule with a diameter of 10 mm.

a. Standard chest radiograph. There is a simulated nodule overlapped by the rib shadow in the right upper lung field (arrow).

b. Soft-tissue image produced with the DES technique. The nodule is seen more clearly on the DES image. The mean rating score of all observers was increased from 56.2 to 80.6 by using the DES image.

Table 1: AUC values for all observers for the detection of simulated nodules without and with DES images

	AUC value	
Observer	Without DES images	With DES images
1	0.74	0.77
2	0.71	0.82
3	0.79	0.82
4	0.86	0.87
5	0.83	0.84
6	0.74	0.80
7	0.63	0.66
Mean ± SD	0.76 ± 0.08	0.79 ± 0.07

AUC, The area under the best-fit ROC curve; DES, dual-energy subtraction; SD, standard deviation

Table 2: Results of nodule detection for all observers without and with DES images

	Sensitivity (%)	Specificity (%)	Accuracy (%)	PPV (%)	NPV (%)
All nodules					
Standard image	48.8	83.6	65.4	79.5	58.9
DES image	63.2*	83.6	73.4*	82.6	70.6*
Nodules with -450 HU					
Standard image	39.7	81.7	60.7	71.2	57.8
DES image	52.4	84.1	68.3*	81.1	65.4
Nodules with -200 HU					
Standard image	51.6	85.7	68.7	84.0	63.5
DES image	55.6	85.7	70.6	88.4	67.1
Nodules with 30 HU					
Standard image	76.2	83.3	79.8	81.6	79.2
DES image	80.2	81.0	80.6	81.8	82.1

*Statistically significant difference compared with the value of the corresponding standard image

PPV, positive predictive value; NPV, negative predictive value; DES, dual-energy subtraction